Tonotopy of the mammalian cochlea is associated with stiffness and tension gradients of the hair cell's tip-link complex.

Mélanie Tobin[1,2], Vincent Michel[2,3,4], Nicolas Michalski[2,3,4], Pascal Martin[1,2,*]

[1] Laboratoire Physico-Chimie Curie, Institut Curie, PSL Research University, CNRS, UMR168, F-75248 Paris, France.

[2] Sorbonne Université, F-75252 Paris, France

[3] Laboratoire de Génétique et Physiologie de l'Audition, Institut Pasteur, Paris, France.

[4] UMRS 1120, Institut National de la Santé et de la Recherche Médicale (INSERM), Paris, France.

[*] Correspondence: pascal.martin@curie.fr

ABSTRACT [150 words] Frequency analysis of sound by the cochlea relies on sharp frequency tuning of mechanosensory hair cells along a tonotopic axis. To clarify the underlying biophysical mechanism, we have investigated the micromechanical properties of the hair cell's mechanoreceptive hair bundle in the rat cochlea. We studied both inner and outer hair cells, which send nervous signals to the brain and amplify cochlear vibrations, respectively. We find that tonotopy is associated with gradients of stiffness and resting mechanical tension, with steeper gradients for outer hair cells, emphasizing the division of labor between the two hair-cell types. We demonstrate that tension in the tip links that convey force to the mechano-electrical transduction channels increases at reduced Ca^{2+}. Finally, we reveal tonotopic gradients in stiffness and tension at the level of a single tip link. We conclude that intrinsic mechanical gradients of the tip-link complex help specify the characteristic frequency of the hair cell.

INTRODUCTION

The cochlea –the auditory organ of the inner ear– is endowed with a few thousands of mechanosensory hair cells that are each tuned to detect a characteristic sound frequency (Fettiplace and Kim, 2014). Different frequencies are detected by different cells, which are spatially distributed in the organ according to a frequency –or tonotopic– map (Lewis et al., 1982; Greenwood, 1990; Viberg and Canlon, 2004). Despite its critical importance for frequency analysis of complex sound stimuli, determining the mechanism that specifies the characteristic frequency of a given hair cell remains a major challenge of auditory physiology.

Although certainly not the only determinant of hair-cell tuning (Fettiplace and Fuchs, 1999), we focus here on the contribution of the hair bundle, the cohesive tuft of cylindrical processes called stereocilia that protrude from the apical surface of each hair cell. The hair bundle works as the mechanical antenna of the hair cell (Hudspeth, 1989). Sound evokes hair-bundle deflections, which modulate tension in oblique proteinaceous tip links (Pickles et al., 1984; Kazmierczak et al., 2007) that interconnect the stereocilia near their tips. A change in tip-link tension affects the open probability of mechanosensitive ion channels, resulting in a mechano-electrical transduction current. The operating point of the transducer lies within the steep region of the sigmoidal relation between the transduction current and the hair-bundle position (Corey and Hudspeth, 1983; Russell and Sellick, 1983; Johnson et al., 2011). This key condition for sensitive hearing is thought to be controlled by tension in the tip links at rest (Hudspeth and Gillespie, 1994; Gillespie and Muller, 2009), as well as by extracellular and intracellular calcium (Corey and Hudspeth, 1983; Ricci et al., 1998; Fettiplace and Kim, 2014), which is thought to stabilize the closed state of the transduction channels (Hacohen et al., 1989; Cheung and Corey, 2006). Tip-link tension has been estimated at ~8 pN in the bullfrog's sacculus (Jaramillo and Hudspeth, 1993) but, to our knowledge, there has been no such report in the mammalian cochlea.

Adaptation continuously resets the mechanosensitive channels to a sensitive operating point when static deflections of the hair bundle threaten to saturate mechanoelectrical transduction (Eatock, 2000). Most of the available evidence indicates that movements by molecular motors actively pulling on the tip links and calcium feedback on the open probability of transduction channels contribute to adaptation. With mammalian cochlear hair cells, however, the dependence of adaptation on Ca^{2+} entry has recently been the subject of significant controversy (Peng et al., 2013; Corns et al., 2014; Peng et al., 2016; Effertz et al., 2017). Motor forces and calcium feedback can also explain the active hair-bundle

movements, including spontaneous oscillations, that have been observed in various species (Fettiplace and Hackney, 2006; Martin, 2008). Active hair-bundle motility may contribute to hair-cell tuning by actively filtering and amplifying sound inputs (Hudspeth, 2008). These findings emphasize the importance of the tip-link complex (Michalski and Petit, 2015) –a protein assembly which includes the transduction channels, the tip links that convey sound-evoked forces to these channels, as well as the molecular motors that pull on the tip links– for mechanosensitivity of the hair cell.

Electrophysiological properties of the transduction apparatus, including the activation kinetics and the conductance of the transduction channels, as well as the kinetics of adaptation, have been shown to vary with the characteristic frequency of the hair cell (Ricci et al., 2003; Ricci et al., 2005; Fettiplace and Kim, 2014; Beurg et al., 2018). These observations suggest that hair-cell tuning may depend on the transducer itself (Ricci et al., 2005). In addition, it is a ubiquitous property of vertebrate auditory organs that the morphology of the hair bundle varies systematically with the characteristic frequency of the corresponding hair cell (Wright, 1984; Lim, 1986; Roth and Bruns, 1992; Tilney et al., 1992): going from the high-frequency to the low-frequency region of the organ, the hair bundle gets longer and comprises a progressively smaller number of stereocilia. These morphological gradients have long been recognized as circumstantial evidence that the mechanical properties of the hair bundle might be involved in frequency tuning (Turner et al., 1981; Flock and Strelioff, 1984; Fettiplace and Fuchs, 1999). However, a detailed characterization of mechanical gradients at the level of the whole hair bundle is lacking, in particular to clarify the contribution of the tip-link complex to these gradients.

In this work, we probed passive and active hair-bundle mechanics along the tonotopic axis of an excised preparation of the rat cochlea (Fig. 1). We worked both with inner hair cells, which convey auditory information to the brain and are considered as the true sensors of the organ, and outer hair cells, which are mostly dedicated to cochlear amplification of sound-evoked vibrations (Hudspeth, 2014). We combined fluid-jet stimulation to deflect the hair bundle, iontophoresis of a calcium chelator (EDTA) to disrupt the tip links and measure bundle movements resulting from tension release by these links, and patch-clamp recordings of transduction currents to infer the number of intact tip links contributing to the response. From these measurements, we estimated the stiffness of the whole hair bundle, the contribution of the tip links and of the stereociliary pivots to this stiffness, as well as the resting tension in the tip links. Our results reveal mechanical gradients of the tip-link

complex according to the tonotopic map and to the division of labor between sensory inner and amplificatory outer hair cells, providing evidence for the implication of the tip-link complex to frequency tuning of cochlear hair cells.

RESULTS

The hair-bundle stiffness increases along the tonotopic axis. Using a calibrated fluid jet (Methods; Figure 2–supplementary text; Figure supplements 1-4), we measured the stiffness of single hair bundles along the tonotopic axis of the rat cochlea, going from the very apex of the organ to mid-cochlear locations (Fig. 1). For outer hair cells, we found that a given series of force steps evoked hair-bundle deflections that decreased in magnitude towards more basal locations along the tonotopic axis (Fig. 2A). Correspondingly, the slope of a bundle's force-displacement relation (Fig. 2B), and thus stiffness, increased with the characteristic frequency of the hair cell. The same behavior was observed for inner hair cells (Fig. 2C-D). Remarkably, the stiffness gradient was steeper (*$p<0.05$; Figure 2–table supplement 1) for outer hair cells than for inner hair cells (Fig. 2E). As the characteristic frequency increased from 1 to 4 kHz, the hair-bundle stiffness K_{HB} showed a 3.4-fold increase from 3.7±0.3 mN/m (n = 19) to 12.7±0.7 mN/m (n = 21) for outer hair cells, but only a 2.2-fold increase from 2.6±0.3 mN/m (n = 19) to 5.7±0.6 mN/m (n = 19) for inner hair cells. At the 15-kHz position, where stiffness could only be recorded for inner hair cells (see Methods), K_{HB} = 8.2±0.6 mN/m (n = 14), thus still significantly lower (***$p<0.001$; Figure 2–table supplement 1) than in outer hair cells at the 4-kHz position. At each cochlear position, outer hair-cell bundles were stiffer than inner hair-cell bundles, with a stiffness ratio that increased from the apex to the base of the organ.

Parsing out the relative contributions of gating springs and stereociliary pivots to hair-bundle stiffness. There are two contributions to the stiffness of a hair bundle: $K_{HB} = K_{GS} + K_{SP}$. First, hair-bundle deflections modulate the extension of elastic elements –the gating springs that control the open probability of the mechano-electrical transduction channels; we denote by K_{GS} their contribution to hair-bundle stiffness. Second, bending of the actin core of the stereocilia at the stereociliary pivots, as well as stretching horizontal lateral links that interconnect the stereocilia, provides the remaining contribution K_{SP}. Because the gating springs are in series with the tip links, disrupting the tip links affords a means to estimate both K_{GS} and K_{SP}. We used local iontophoretic application of a Ca^{2+} chelator (EDTA; Methods and Fig. 1) to disengage the Ca^{2+}-dependent adhesion of the cadherin-related molecules

forming each tip link (Kazmierczak et al., 2007). From the increased magnitude of the hair-bundle response to a given mechanical stimulus (see an example in Fig. 4A), we found that the gating springs contributed up to 50% of the total hair-bundle stiffness K_{HB}. Averaging over all inner and outer hair cells that we tested, the relative contribution of the gating springs was $r = K_{GS}/K_{HB} = 22\pm2$ % (n = 71; Figure 3–figure supplement 1), where $1 - r$ is the amplitude ratio of hair-bundle movements before and after tip-link disruption. Both inner and outer hair cells displayed a gradient of gating-spring stiffness $K_{GS} = r\,K_{HB}$ (Fig. 3A). Between the 1-kHz and the 4-kHz positions, the 6.6-fold increase that we measured for outer hair cells was significantly larger (**p<0.01; Figure 3–table supplement 2) than the 3.7-fold increase observed for inner hair cells. Similarly, the contribution $K_{SP} = (1 - r)\,K_{HB}$ of the stereociliary pivots to hair-bundle stiffness displayed tonotopic gradients for both inner and outer hair cells (Fig. 3B).

Individual gating springs are stiffer in hair cells with higher characteristic frequencies. Both the pivot stiffness K_{SP} and the gating-spring stiffness K_{GS} are expected to vary according to hair-bundle morphology. Hair bundles get shorter and are composed of more numerous stereocilia as one progresses from the apex to the base of the cochlea (Figure 3–figure supplement 2), which ought to promote higher stiffness values. Are morphological gradients sufficient to explain the observed stiffness gradients of the hair bundle? Accounting for morphology, we write $K_{SP} = \kappa\,N_{SP}/\,h^2$ and $K_{GS} = k_{GS}\,N_{TL}\gamma^2$, in which h, N_{SP}, N_{TL} correspond, respectively, to the height, the number of stereocilia and the number of (intact) tip links of the hair bundle, whereas $\gamma \propto 1/h$ is a geometrical projection factor (Figure 3–figure supplements 1-3). Remarkably, the intrinsic rotational stiffness κ of a single stereocilium in outer hair cells remained the same across the positions that we explored (Fig. 3C; Figure 3–table supplement 2). Similarly, with inner hair cells, there was no significant variation of the rotational stiffness between the 1- and 2-kHz locations as well as between the 4- and 15-kHz locations, although we observed a 2-fold stiffness increase between the 2- and 4-kHz locations (Figure 3–table supplement 2). Averaging over the ensembles of outer and inner hair cells that we probed, the rotational stiffness $\kappa = 1.8\pm0.2$ fN·m/rad (n = 78) in outer hair cells was about 2.5-fold higher than the value $\kappa = 0.8\pm0.1$ fN·m/rad (n = 136) measured in inner hair cells. In contrast, the intrinsic stiffness k_{GS} of a single gating spring increased 2.9 fold from 1.9±0.5 (n = 20) to 5.5±0.7 mN/m (n = 30) in outer hair cells and 3.6 fold from 0.7±0.1 (n = 44) to 2.5±0.4 mN/m (n = 21) in inner hair cells, for characteristic frequencies that increased from 1 to 4 kHz and from 1 to 15 kHz, respectively (Fig. 3D). Thus,

morphological gradients can account for the observed gradient in pivot stiffness K_{SP}, but not for the observed gradient in gating-spring stiffness K_{GS} and in turn for the whole hair-bundle stiffness K_{HB}. The hair-bundle morphology is not the sole determinant of hair-bundle mechanics.

Tip-link tension increases along the tonotopic axis. We then estimated the resting mechanical tension in the tip links, *i.e.* in the absence of an external stimulus. The transduction channels close when the tip links are disrupted, indicating that the channels are inherently more stable in a closed state (Assad et al., 1991; Beurg et al., 2008; Indzhykulian et al., 2013). In functional hair bundles, tip-link tension is thought to bring the operating point of the transducer within the steep region of the sigmoidal relation between the channels' open probability and the position of the hair bundle, ensuring sensitive detection of hair-bundle deflections. If there is tension in the tip links, then disrupting these links must result in a positive offset in the resting position of the hair bundle (Assad et al., 1991; Jaramillo and Hudspeth, 1993).

In response to iontophoresis of a Ca^{2+} chelator (EDTA), we observed a net positive movement ΔX_R of the hair bundle at steady state, as expected if the tip links broke and released tension (Fig. 4A). Consistent with tip-link disruption, this movement was associated with a decrease in hair-bundle stiffness, as well as with closure of the transduction channels and loss of transduction (Fig. 4B). The positive offset in resting position upon tip-link disruption was observed at all positions that we explored along the tonotopic axis of the cochlea, both for inner and outer hair cells, demonstrating that the hair bundles were indeed under tension (Fig. 5A). In addition, we observed that the magnitude of the evoked movement increased significantly (**$p<0.01$; Figure 5–table supplement 1) from 9±3 nm ($n = 13$) to 45±10 nm ($n = 12$) for outer hair cells with characteristic frequencies that increased from 1 to 4 kHz. In contrast, we observed no significant difference among inner hair cells with characteristic frequencies that varied within the 1−15-kHz range ($p>0.05$; Figure 5–table supplement 1): the positive offset was 21±2 nm ($n = 71$) over the whole ensemble of inner hair cells.

As a result, within the range of cochlear locations that we explored, we measured a steep gradient of hair-bundle tension for outer hair cells but a comparatively weaker gradient (*$p<0.05$; Figure 5–table supplement 1) for inner hair cells (Fig. 5B). Tension $T_R = K_{SP}\,\Delta X_R$ in the hair bundle was estimated as the product of the pivot stiffness K_{SP} and the positive offset ΔX_R in resting position evoked by tip-link disruption (Methods). The hair-bundle

tension showed a 13.6-fold increase from 27±10 pN (n = 14) to 366±87 pN (n = 16) for outer hair cells (characteristic frequencies: 1−4 kHz) but only a 4.1-fold increase from 37±7 pN (n = 31) to 149±33 pN (n = 11) for inner hair cells (characteristic frequencies: 1−15 kHz). Tension in the hair bundle resulted from the summed contributions of tension in individual tip links. Dividing the tension T_{R} by the average number N_{TL} of intact tip links in our recordings and projecting the result along the oblique axis of the tip links (projection factor γ) provided estimates of the tension $t_{\mathrm{R}} = T_{\mathrm{R}}/(\gamma\, N_{\mathrm{TL}})$ in a single tip link. Remarkably, the observed gradients in hair-bundle tension (Fig. 5B) were not only due to an increase in the number of tip links that contributed to this tension (Figure 3−figure supplement 3), for tension in a single tip link also showed gradients (Fig. 5C). The single tip-link tension was comparable in the two types of cells at the 1-kHz location: 6.9±2.9 pN (n = 22) for outer hair cells and 9.0±1.9 pN (n = 42) for inner hair cells. However, at the 4-kHz location, the single tip-link tension had increased 7.2 fold to 50±12 pN (n = 18) in outer hair cells but only 2.7 fold to 24±6 pN (n = 16) in inner hair cells; at the 15-kHz location, tip-link tension in inner hair cells was 28±7 pN (n = 17). A linear regression of the relation between the single tip-link tension and the characteristic frequency confirmed that the gradient was significantly (*$p<0.05$; Figure 5−table supplement 1) steeper for outer hair cells.

Tip-link tension first increases upon Ca^{2+} chelation. The dynamic response to an iontophoretic step of EDTA, and thus to a decrease of the extracellular Ca^{2+} concentration, was biphasic. The hair bundle first moved in the negative direction (arrowhead in Fig. 4A), before the directionality of the movement reverted and the bundle showed the positive movement associated with tip-link disruption. The negative movement was associated with an increased inward current of similar time course (Fig. 4B). Within the framework of the gating-spring model of mechanoelectrical transduction (Corey and Hudspeth, 1983; Markin and Hudspeth, 1995), this observation is readily explained if the evoked decrease in the extracellular Ca^{2+} concentration resulted in an increase in gating-spring tension, which both pulled the hair bundle in the negative direction and led to the opening of the transduction channels.

The magnitude of the negative movement at the peak showed no significant gradient and was similar between inner and outer hair cells, with an average magnitude of $\Delta X_{\mathrm{Ca}} = -26\pm2$ nm over the whole ensemble of hair cells (n = 83; Fig. 6A). However, because morphological gradients (Figure 3−figure supplement 2) resulted in gradients of pivot stiffness $\mathrm{K_{SP}}$ (Fig. 3B), the maximal increase $\Delta T = -\mathrm{K_{SP}}\,\Delta X_{\mathrm{Ca}}$ in hair-bundle tension was

larger for hair cells with higher characteristic frequencies (Fig. 6B), as was the maximal tension $t_{\max}$ that a single tip link sustained before tip-link disruption (Fig. 6C). Going from 1-kHz to 4-kHz locations, this maximal tip-link tension displayed a gradient from 21±6 pN (n = 29) to 80±17 pN (n = 22) in outer hair cells and from 23±4 pN (n = 42) to 66±11 pN (n = 16) in inner hair cells; at the 15-kHz location, the maximal tension was not significantly different than at the 4-kHz location in inner hair cells.

When immersing the hair cells in low-Ca^{2+} saline, the negative movement was always followed by tip-link disruption and could thus not be observed twice with the same hair bundle. However, in six different preparations for which the hair bundle was immersed in saline with a higher Ca^{2+} concentration (500 µM) than usual (20 µM), we were able to preserve the integrity of the tip links and demonstrate that the negative movements could be reversible (Fig. 6D). Under such conditions, we observed that the absolute magnitude and the speed of the negative movement increased with the magnitude of the iontophoretic current. Notably, the hair bundle reached a new steady-state position when the iontophoretic step was long enough (Fig. 6E), suggesting that resting tension in the tip links could be modulated by the extracellular Ca^{2+} concentration, with higher tensions at lower Ca^{2+} concentrations.

DISCUSSION

Tonotopy of the mammalian cochlea is known to be associated with gradients of hair-bundle morphology (Wright, 1984; Lim, 1986; Roth and Bruns, 1992; Tilney et al., 1992), as well as of electrophysiological properties of the transduction apparatus (Ricci et al., 2003; Ricci et al., 2005; Fettiplace and Kim, 2014; Beurg et al., 2018). The work presented here reveals that tonotopy is also associated with gradients of intrinsic mechanical properties of the hair cell's tip-link complex. Specifically, by dissecting the relative contributions of the tip links and of the stereociliary pivots to the micromechanical properties of the hair bundle, we found that the gating springs that control the open probability of the mechanoelectrical transduction channels are stiffer (Fig. 3D) and subjected to higher mechanical tension (Fig. 5C) in hair cells that respond to higher characteristic frequencies. In return, our data suggests that the tip-link complex plays a mechanical role in the complex process that sets the characteristic frequency of the hair cell.

The stiffness K_{HB} of the whole hair bundle displayed steeper gradients than those expected using the rough estimate $K_{HB} \propto N_{SP}/h^2$ from morphological changes (Figure 3–figure supplement 2) in length h and number of stereocilia N_{SP}. Computing the relative difference in stiffness ratio between the two extreme cochlear locations that we were able to probe, we

roughly estimate that the measured stiffness ratios (Fig. 2E) were 51% and 66% larger than those expected from morphology for outer and inner hair cells, respectively. We interpret this result as the consequence of intrinsic gradients of the single gating-spring stiffness (Fig. 3D). Further emphasizing mechanical regulation at the level of the tip-link complex, we also observed that the rotational stiffness of a single stereocilium was nearly uniform across the cochlear locations that we tested, especially in outer hair cells (Fig. 3C). Stiffness gradients of hair bundles with disrupted tip links are thus entirely determined by morphology, in contradistinction to intact hair bundles.

Our experiments were performed with hair cells from juvenile animals (P7-P10), before the onset of hearing. Hair-cell maturation progresses from base to apex in the cochlea (Wu and Kelley, 2012), which may thus have affected our estimates of mechanical gradients of the tip-link complex. However, because 92% percent of our recordings were performed at P8 or later (Methods), the tip-link complex ought to be nearly mature in our experiments, at least in outer hair cells (Roth and Bruns, 1992; Waguespack et al., 2007; Beurg et al., 2018). In inner hair cells, we cannot exclude that maturation of the hair-bundle morphology was still proceeding at the most apical cochlear positions explored in our study (Peng et al., 2009). Maturation sharpens the apex-to-base gradient of bundle length (Roth and Bruns, 1992); based on bundle morphology only, we would expect to underestimate stiffness gradients with immature inner hair cells.

How stiffness gradients may contribute to the tonotopic map. We observed a ~3.4-fold increase of hair-bundle stiffness over two octaves (1–4 kHz) of characteristic frequencies for outer hair cells and a similar increase but over 4 octaves (1–15 kHz) for inner hair cells (Fig. 2E). Whether or not stiffness would continue increasing along the same gradient towards more basal locations of the cochlea is unknown. If it were the case, we would expect a base-to-apex stiffness ratio of ~40 for outer hair cells, which is comparable to the base-to-apex ratio of characteristic frequencies in the rat cochlea (range: 0.5-50 kHz; (Viberg and Canlon, 2004)), but only of ~6 for inner hair cells. The interplay between the stiffness and mass of a hair bundle could in principle help specify the preferred frequency of vibration of the hair cell through passive mechanical resonance with sound stimuli (Frishkopf and DeRosier, 1983; Holton and Hudspeth, 1983; Manley et al., 1988; Freeman and Weiss, 1990; Gummer et al., 1996). The resonance frequency $\omega_C = \sqrt{k/m}$ of a spring-mass system is given by the square root of the system's stiffness k divided by the mass m; it thus increases with stiffness, but relatively slowly. Assuming for simplicity that the bundle's mass remains

nearly the same along the tonotopic axis (Tilney and Tilney, 1988), two orders of magnitude in frequency must be produced by a 10,000-fold increase in stiffness, corresponding to much steeper gradients than those reported here.

Alternatively, it has been proposed that the hair bundle could actively resonate with sound as the result of spontaneous oscillations (Martin et al., 2001; Hudspeth, 2008). Within this framework, the characteristic frequency is set by the frequency of the oscillator, which is expected to increase with the stiffness of the hair bundle (Vilfan and Duke, 2003; Tinevez et al., 2007; Martin, 2008; Barral et al., 2018). Notably, the relation may be steeper than that resulting from a passive spring-mass system, possibly approximating a linear dependence (Hudspeth et al., 2010). In this case, the stiffness gradient observed here (Fig. 2E) for outer hair cells, but not for inner hair cells, could be steep enough to be a major determinant of the tonotopic map.

Functional role of tension gradients. Tip-link tension is thought to control the open probability of the transduction channels, with higher tension promoting opening of the channels (Hudspeth and Gillespie, 1994). On this basis, a gradient of tip-link tension (Fig. 5C) ought to result in a gradient of open probability. Yet, it has been shown in outer hair cells that the channels' open probability –the operating point of the transducer– remains remarkably uniform along the tonotopic axis, near a value of ½ (Johnson et al., 2011). To explain this observation, we note that the tension gradient for outer hair cells is associated with a gradient of single-channel conductance (Beurg et al., 2006; Beurg et al., 2015; Beurg et al., 2018). As a consequence, the magnitude of the Ca^{2+} influx into transducing stereocilia is expected to increase with the characteristic frequency of the hair cell. Manipulations that affect the extracellular or the intracellular Ca^{2+} concentration indicate that the transduction channels close at increased Ca^{2+} concentrations (reviewed in (Fettiplace and Kim, 2014)), possibly because the channels are harder to open when the Ca^{2+} concentration is higher near the channel's pore (Cheung and Corey, 2006). Thus, the gradient of tip-link tension reported here (Fig. 5C) may compensate for the effects of the conductance gradient on the open probability: channels with higher conductance impart higher Ca^{2+} influxes (closing the channels) but are also subjected to higher tension (opening the channels), perhaps maintaining an optimal operating point for the transducer at all cochlear locations.

Tension in the tip links is thought to be produced actively by pulling forces from molecular motors interacting with the actin core of the stereocilia at the upper insertion point of the tip link (Gillespie and Muller, 2009). The observed tension gradient in turn implies that, towards

basal cochlear locations, there are more motors or that each motor exerts higher forces than near the apex. Notably, the tip links of inner-hair-cell bundles were found to bear less tension than those of outer hair cell (Fig. 5B-C). This property qualitatively makes sense, for the open probability of the transduction channels is thought to be smaller in inner hair cells than in outer hair cells (Russell and Sellick, 1983). There is also no, or only a weak, gradient of the single-channel conductance in inner hair cells (Beurg et al., 2006; Beurg et al., 2018), which parallels the relatively weak gradient of tip-link tension observed here.

Tip-link tension may be high enough to alter tip-link conformation and affect gating-spring stiffness. The tip link is composed of the association of two cadherin-related proteins, cadherin-23 and protocadherin-15 (PCDH15) (Kazmierczak et al., 2007). Molecular dynamics simulations have suggested that a bend between extracellular cadherin (EC) repeats 9 and 10 of PCDH15 may confer some compliance to otherwise rigid tip links (Araya-Secchi et al., 2016). Tensions higher than ~10 pN are predicted to evoke complete unbending of EC9-10, resulting in significant stiffening of the tip link. Assuming that PCDH15 in the tip link forms a dimer (Kazmierczak et al., 2007; Ge et al., 2018) and that tip-link tension is equally shared by the two filaments, our estimates of tip-link tension (Fig. 5C) are compatible with a contribution of the bending elasticity of EC9-10 to gating-spring stiffness at the apex of the rat cochlea, especially in inner hair cells. In outer hair cells, as one progresses from the very apex towards more basal cochlear locations, tension may quickly become too high to allow a bent conformation in EC9-10. At the 4-kHz location, we estimated a resting tip-link tension of ~50 pN. Taking the measured unfolding forces of Ig domains in titin as a reference (Rief et al., 1997), tip-link tension might actually be high enough to evoke unfolding of EC domains, at least under resting conditions or at physiological loading rates. Whether or not unfolding a various number of EC domains can contribute to a gradation of gating-spring stiffness remains to be explored (Bartsch and Hudspeth, 2018).

Notably, the estimated gradients of gating-spring tension (Fig. 5C) were associated with gradients of gating-spring stiffness (Fig. 3D): stiffer gating springs are subjected to more resting tension. Strain stiffening is a common phenomenon associated with the entropic elasticity of macromolecules as well as with filamentous protein networks (Bustamante et al., 1994; Rief et al., 1997; Kang et al., 2009). A tension gradient may thus in part explain the existence of the observed gradient of gating-spring stiffness. Alternatively, the gating-spring stiffness could vary if the gating spring were composed of a variable number of compliant molecules operating in parallel and connected to a single tip link. Consistent with this

hypothesis, it has recently been suggested that the number of TMC1-dependent transduction channels increases by ~2.5-fold in outer hair cells but shows nearly no gradient in inner hair cells from the apex to the base of the mouse cochlea (Beurg et al., 2018). If each channel were associated with its own gating spring, the number of transduction channels per tip link would directly control the effective stiffness of the tip-link complex. This mechanism could contribute to the stiffness gradients reported here (Fig. 3D). However, for outer hair cells, we found that the stiffness of the tip-link complex increased by ~3-fold over a region spanning only 20% of the cochlear tonotopic axis (Fig. 3D), whereas the conductance associated with a single tip-link varies by a similar amount over the whole cochlear length (Beurg et al., 2006; Beurg et al., 2018). Thus, if there is a relation between stiffness and conductance of a single tip-link complex, this relation cannot simply be proportional.

Tip-link tension depends on calcium. Upon iontophoretic application of a Ca^{2+} chelator (EDTA), before tip-link disruption, we observed that the hair bundle first moved in the negative direction and that this movement was associated with a concomitant opening of the transduction channels (Fig. 4). Calcium acts as a permeant channel blocker of the transduction channels (Fettiplace and Kim, 2014). Lowering the extracellular Ca^{2+} concentration is thus expected to increase the magnitude of the current flowing through open transduction channels but not to produce hair-bundle movements, at least as the result of block release only. A decrease of the extracellular Ca^{2+} concentration also promotes opening of the transduction channels (Hacohen et al., 1989; Johnson et al., 2011). Within the framework of the gating-spring model of mechanoelectrical transduction, channel opening must reduce gating-spring extension and in turn tension, fostering *positive* movements of the hair bundle. Thus, the observed *negative* movements cannot result from internal forces associated with channel gating. Instead, our observations are readily explained if the evoked reduction of extracellular Ca^{2+} concentration resulted in an increase of tip-link (and thus gating-spring) tension. If tip-link tension at rest is set by myosin molecular motors that pull on the tip links (Hudspeth and Gillespie, 1994), then the motor force must increase at decreased Ca^{2+} concentrations.

Interestingly, depolarization of rat outer hair cells was previously shown to evoke positive movements of the hair bundle (Kennedy et al., 2006). Both depolarization and chelation of extracellular Ca^{2+} are expected to reduce the intracellular Ca^{2+} concentration in the vicinity of the transduction channel's pore. Yet, the directionality of active hair-bundle movements is opposite in the two studies, suggesting that the hair bundle can operate in two regimes (Tinevez et al., 2007). In the first regime (Kennedy et al., 2006), the response to Ca^{2+} changes

is dominated by gating forces (Howard and Hudspeth, 1988) so that the resting tension in the tip links is nearly the same before and after application of the stimulus. In the other regime (our study), Ca^{2+}-evoked changes of the resting tension in the tip links (Fig. 6) dominate gating forces. In the chicken cochlea, depolarization of the hair cell was reported to evoke negative movements of the hair bundle (Beurg et al., 2013), a directionality in agreement with that found here (Fig. 4A). In addition, it has been shown in the bullfrog's sacculus (Tinevez et al., 2007) and the turtle's cochlea (Ricci et al., 2002) that the response of different hair cells to a given Ca^{2+} change can be of either directionality and that the directionality of the response for a given hair cell can even be reversed by applying a position offset to the hair bundle. The two regimes of active hair-bundle motility can thus potentially coexist within the same hair cell, but only if gating forces are strong enough (Tinevez et al., 2007). We measured force-displacement relations that were remarkably linear (Fig. 2B and D), showing no sign of gating compliance (Howard and Hudspeth, 1988). This observation confirms that gating forces were relatively weak under our experimental conditions, although others have shown that gating compliance can be measured with mammalian cochlear hair cells (Russell et al., 1992; Kennedy et al., 2005).

The effect of Ca^{2+} on mechanoelectrical transduction has recently been the subject of significant debate and controversy (Peng et al., 2013; Corns et al., 2014). We showed here that the response of rat cochlear hair bundles to iontophoretic Ca^{2+} changes are remarkably similar to that reported with hair cells from non-mammalian vertebrates (Jaramillo and Hudspeth, 1993): tip-link tension depends on the extracellular Ca^{2+} concentration, giving rise to active hair-bundle movements in response to Ca^{2+} changes (Figs. 4 and 6).

Mechanical gradients reflect the division of labor between inner and outer hair cells. Stiffness (Fig. 2E) and tension (Fig. 5B) gradients were steeper for outer hair cells, which serve primarily as mechanical amplifiers of sound-evoked vibrations, than for inner hair cells, the true sensors of the inner ear. Other properties, such as the height of the hair bundle (Wright, 1984; Lim, 1986; Roth and Bruns, 1992) or the conductance of the transduction channels (Beurg et al., 2006; Beurg et al., 2018), show a similar behavior. These observations suggest that cochlear amplification near a characteristic frequency imposes stringent constraints on the tip-link complex of outer hair cells. Consequently, our data fosters the hypothesis that the hair bundle and its transduction machinery are involved in this active process (Hudspeth, 2014).

METHODS

Experimental preparation. All experimental procedures were approved by the Ethics committee on animal experimentation of the Institut Curie; they complied with the European and French-National Regulation for the Protection of Vertebrate Animals used for Experimental and other Scientific Purposes (Directive 2010/63; French Decree 2013-118). Experiments were performed on excised cochlear coils of Sprague Dawley rats (Janvier Labs) between postnatal day 7 and 10 (P7–P10), with 8% of the cells at P7, 75% at P8–P9 and 17% at P10. The dissection of the cochlea followed a published procedure (Kennedy et al., 2003). In short, we cracked open the bony shell covering the cochlear tissue, unwound the cochlear tube from the modiolus, removed the stria vascularis, and gently peeled the tectorial membrane. Apical or middle turns of the organ of Corti were positioned under strands of nylon fibres in the experimental chamber. We recorded from inner hair cells at 4 positions along the longitudinal axis of the cochlea (Fig. 1A), corresponding to fractional distances of 5%, 10%, 20%, and 50% from the cochlear apex. According to the tonotopic map in this species (Viberg and Canlon, 2004), these cells were tuned at characteristic frequencies of 1, 2, 4, and 15 kHz, respectively. We also recorded from outer hair cells but only at the first three positions along the tonotopic axis. Farther towards the cochlear base, the hair bundles were too small to be clearly visualized and mechanically stimulated.

The tissue was bathed in a standard saline containing 150 mM NaCl, 6 mM KCl, 1.5 mM $CaCl_2$, 2 mM Na-pyruvate, 8 mM glucose and 10 mM Na-HEPES. In some experiments, we used a low-Ca^{2+} saline containing 150 mM NaCl, 6 mM KCl, 3.3 mM $CaCl_2$, 4 mM HEDTA, 2 mM Na-pyruvate, 8 mM glucose, and 10 mM Na-HEPES. As measured with a Ca^{2+}-sensitive electrode, this solution had a free Ca^{2+} concentration of 22 µM, similar to that found in rat endolymph (Bosher and Warren, 1978). All solutions had a pH of 7.4 and an osmotic strength of 315 $mOsm \cdot kg^{-1}$. Experiments were performed at a room temperature of 20–25°C.

Microscopic Apparatus. The preparation was viewed through a ×60 water-immersion objective of an upright microscope (BX51WI, Olympus). Individual hair bundles were imaged at a magnification of ×1,000 onto a displacement monitor that included a dual photodiode. Calibration was performed before each recording by measuring the output voltages of the monitor in response to a series of offset displacements of the photodiode. For hair-bundle movements that did not exceed ±150 nm in the sample plane, the displacement monitor was linear.

Iontophoresis of a Ca^{2+} Chelator. We used iontophoresis to apply the calcium chelator EDTA in the vicinity of a hair bundle (Fig. 1B) and disrupt its tip links (Assad et al., 1991; Jaramillo and Hudspeth, 1993; Marquis and Hudspeth, 1997). Coarse microelectrodes were fabricated from borosilicate capillaries with a pipette puller (P97, Sutter Instrument); their resistance was 1 MΩ when filled with 3 M KCl and immersed in the same solution. In experiments, the electrodes were filled with a solution containing 100 mM EDTA and 25 mM KCl. The electrode's tip was positioned at ~3 μm from the hair bundle. A holding current of +10 nA was continuously applied to counteract the diffusive release of EDTA from the electrode. The stimulus consisted of a –100-nA current step on top of the holding current, resulting in a net iontophoretic current of –90 nA. To facilitate tip-link disruption upon EDTA iontophoresis, the cochlear tissues were immersed in low-Ca^{2+} saline (~20-μM Ca^{2+}).

Mechanical stimulation and stiffness measurements. The hair bundles of inner and outer hair cells were mechanically stimulated using a fluid-jet device (Kros et al., 1992; Géléoc et al., 1997; Johnson et al., 2011). Pipettes were pulled from borosilicate glass (TW150-F, World Precision Instruments); their tip diameter was adjusted within a range of 5–10 μm. Fluid flow through a pipette was driven by a voltage command to a piezoelectric disk (Murata 7BB-27-4). Any steady-state flow coming in or out of the pipette was nulled by changing the hydrodynamic pressure inside the fluid-jet pipette; the hydrodynamic pressure was adjusted with a syringe connected to the body of the fluid-jet device. The fluid-jet pipette was positioned on the abneural side of the bundle along the hair bundle's axis of mirror symmetry (Fig. 1C). Fluid coming out the pipette thus deflected the hair bundles towards the shortest stereociliary row, closing the ion channels that mediate mechanoelectrical transduction. This direction of bundle movement is defined as the negative direction in this paper; conversely, positive movements were directed towards the tallest row of stereocilia, fostering opening of the transduction channels. Mechanical stimuli were applied as 100-ms paired-pulse steps (Fig. 2 and Figure 2–figure supplement 3), or 60-Hz sinusoids (Fig. 4) with the magnitude of driving voltages varying between 0 and 60 V.

For stiffness measurements, we measured hair-bundle movements evoked by 100-ms force steps (Fig. 2; see the force-calibration procedure below). We observed that the hair bundle responded to a force step with a fast deflection in the direction of the stimulus followed by a slower movement in the same direction; this mechanical creep was strongly reduced upon tip-link disruption by EDTA treatment (Figure 2–figure supplement 4). Over the duration of the step, the deflection of the hair bundle increased by 12–22% in the direction of the applied

step. The bundle displacement was measured 5–10 ms after the onset of the step stimulus; the stiffness was given by the slope of the relation between the force (noted F in the following) and the displacement of the bundle's tip. These measurements were performed in standard saline.

Applying and measuring forces with the fluid jet. We describe here how we calibrated the hydrodynamic drag force F applied to the hair bundle by a fluid jet by using a flexible glass fiber of known stiffness as a reference. The method is based on a published procedure (Géléoc et al., 1997) that we refined to account for the non-uniform velocity field of the fluid (Figure 2−figure supplement 1). Using a generalized Stokes equation (Leith, 1987), the drag force can be written as $F = 6\pi\eta R_{\mathrm{HB}}\, U$, in which η is the viscosity of the surrounding fluid and R_{HB} is the effective hydrodynamic radius of the bundle. The effective radius R_{HB} was approximated by that of a prolate ellipsoid of short axis h and long axis W, which correspond to the bundle's height and width, respectively. For a fluid flow perpendicular to the axis of rotational symmetry of the ellipsoid, this yields:

$$R_{\mathrm{HB}} \cong 4h/\left\{3\left[\phi/(\phi^2-1) + \left((2\phi^2-3)\ln\left(\phi+\sqrt{\phi^2-1}\right)\right)/(\phi^2-1)^{3/2}\right]\right\}, \quad (1)$$

in which $\phi = W/h$ represents the aspect ratio of the ellipsoid (Happel and Brenner, 2012). Figure 3−table supplement 1 and Figure 3–figure supplement 2 recapitulate the values of parameters h and W that we used to model inner and outer hair-cell bundles along the tonotopic axis of the rat cochlea, as well as the resulting values of R_{HB}. The effective velocity $U \cong \int_{-W/2}^{W/2} v_X(x,y)\, dy/W$ was estimated by computing the mean of the velocity field $v_X(x,y)$ of the fluid over the width W of the hair bundle. Here, $v_X(x,y) = \vec{v}\cdot\vec{e}_X$ is the projection of the fluid velocity $\vec{v}$ on the axis of mechanosensitity (axis X) of the hair bundle; its value is estimated along the axis (Y) perpendicular to axis X for a bundle positioned at a distance x from the mouth of the fluid-jet pipette (Figure 2−figure supplement 1A). Using bead tracers, we found that the velocity profile $v_X(x,y)$ obeyed (Schlichting, 1933)

$$v_X(x,y) = V_{\max}(x)/(1+(y/A(x))^2)^2, \quad (2)$$

where $V_{\max}(x)$ and $A(x)$ characterize, respectively, the maximal speed and the lateral extension of the velocity field at position x (Figure 2−Figure supplement 1B-D). By integrating the velocity profile, we obtain an expression for the force

$$F = 6\pi\eta R_{\mathrm{HB}}\, \beta_{\mathrm{HB}}\, V_{\max} \quad , \quad (3)$$

where $\beta_{HB} = \beta(w) = \frac{1}{2w}(w/(1+w^2) + \tan^{-1} w)$ is a constant that depends on the normalized width of the hair bundle $w = W/(2A)$. Thus, calibrating the force F is equivalent to calibrating the maximal fluid velocity V_{max}.

To estimate V_{max}, we measured the force $\bar{F} \cong 6\pi\eta R_F \bar{U}$ applied by the same jet on a calibrated glass fiber, whose longitudinal axis was oriented perpendicularly to that of the fluid-jet pipette. Given the diameter D_F of the fiber, the effective hydrodynamic radius of a cylindrical fiber was calculated as $R_F = 2L/[3(\ln(L/D_F) + 0.84)]$ (Tirado and Torre, 1979). Because the conical fluid jet intersected the fiber over a length $L > W$, the effective fluid velocity $\bar{U} \cong \int_{-L/2}^{+L/2} v_X(x,y)\, dy/L = \beta_F V_{max}$ for the fiber was smaller than the effective velocity U for the hair bundle, where $\beta_F = \beta(L/(2A)) < \beta_{HB}$. In practice, we used $L(x) = 2\, x\, \tan\alpha + D_{FJ}$, where α is the half-aperture of the conical fluid jet that was visualized using a dye (Coomassie Brilliant Blue; Figure 2–figure supplement 2) and D_{FJ} is the diameter of the mouth of the fluid-jet pipette. We noticed that $L(x) \cong 2A(x)$ (Figure 2–figure supplement 1; figure supplement 2). We used this property to estimate $\beta_{HB} \cong \beta(W/L)$ and $\beta_F \cong \beta(1)$ without having to measure A directly in every experiment.

In experiments, the projected horizontal distance between the tip of the fluid-jet pipette and the hair bundle or the fiber was fixed at $x = 7.8\pm0.3$ µm. Flexible fibers of diameters D_F = 0.7–1.5 µm and stiffness k_F = 0.2–2 mN/m were fabricated and calibrated as described before (Bormuth et al., 2014); their effective hydrodynamic radii varied within a range of $R_F = 2.5$–3.2 µm. A fluid jet of given magnitude elicited a force $\bar{F} = k_F\, \Delta X$, where ΔX is the measured deflection of the fiber. The relation between the force $\bar{F}$ applied to a fiber and the voltage command to the fluid-jet device was linear; its slope provided the calibration constant C (Figure 2–figure supplement 3). When stimulating a hair bundle, a voltage command V_C to the fluid-jet device thus elicited a force $F \cong GCV_C$, where $G = F/\bar{F} = (\beta_{HB}R_{HB})/(\beta_F R_F)$. We used G =1.4±0.1 (mean ± SD; range: 1.27–1.65) for inner hair cells and G =1.3±0.1 (mean ± SD; range: 1.12–1.47) for outer hair cells. Thus, we estimate that the force applied on the hair bundle was 30–40% higher than that measured on the calibration fiber using the same jet of fluid. In practice, we calculated G in each experiment from the geometrical parameters of the fluid-jet pipette, the calibration fiber, and the hair bundle. We noticed that $L(x) \cong 2A(x)$; at a distance $y = L/2$ from the center of the fluid jet ($y = 0$), the fluid velocity is expected to be 25% of the maximal value. Thus, some of the moving fluid was not taken into account in our estimates of the force acting on the fiber, resulting in an

underestimation. However, taking $L(x) = 4A(x)$ resulted in an increase of G by only 5% while the fluid velocity dropped to 4% of the maximal value at the edge of the fluid cone (in $y = L/2 = 2A$).

Electrophysiological recordings. We used the patch-clamp technique to measure mechano-electrical transduction currents. Borosilicate patch pipettes were filled with an intracellular solution containing 142 mM CsCl, 3.5 mM $MgCl_2$, 1 mM EGTA, 5 mM Na_2-ATP, 0.5 mM Na_2-GTP and 10 mM HEPES (pH=7.3, 295 mOsmol/kg). When immersed in standard saline, these pipettes had a resistance of 1.5–3 MΩ. A patch pipette was inserted in the organ of Corti through a pre-formed hole in the reticular lamina and approached parallel to the hair cell rows towards the soma of a target hair cell. During the approach, standard saline was abundantly perfused to protect the Ca^{2+}-sensitive tip-links from EGTA. Hair cells were whole-cell voltage clamped at a holding potential of −80 mV; transduction currents were low-pass filtered at 1-10 kHz (Axopatch 200B; Axon Instruments). No correction was made for the liquid-junction potential. The series resistance was always below 10 MΩ and was compensated up to 70%. To disrupt the tip links with EDTA iontophoresis, the solution bathing the cells was changed to low-Ca^{2+} saline after the cell was patched; the solution change was performed either with a perfusion or with a Picospritzer (Picospritzer III, Parker).

Scanning electron microscopy. Cochleae from P8 rats were processed with osmium tetroxide/thiocarbohydrazide, as previously described (Furness et al., 2008). Samples were analysed by field emission scanning electron microscopy operated at 5 kV (Jeol JSM6700F). The number of stereocilia in inner and outer hair-cell bundles was estimated from electron micrographs at each of the cochlear locations where we performed mechanical and electrophysiological measurements (Figure 3–figure supplement 2; table supplement 1).

Estimating the number of intact tip links in a hair bundle. We performed patch-clamp recordings of the transduction current I_{MAX} elicited at saturation by large hair-bundle deflections (Figure 3–supplement figure 3). In inner hair cells, the number of intact tip links $N_{\mathrm{TL}} = I_{\mathrm{MAX}}/I_1$ was calculated by dividing the saturated current I_{MAX} for the whole hair bundle by the published estimate $I_1 = 35.4$ pA for the transduction current flowing through the tip of a single transducing stereocilium (Beurg et al., 2009); electron microscopy has indeed shown that there is precisely one tip link per stereocilium in an intact hair bundle (Pickles et al., 1984; Kachar et al., 2000). We used the same value of I_1 at all cochlear locations (Beurg et al., 2006; Beurg et al., 2018). Given the magnitude $i = 15$ pA of the current flowing through a single transduction channel, there was on average $I_1/i = 2.36$

transduction channels per transducing stereocilium (Beurg et al., 2006). In outer hair cells, there is no direct estimate of I_1. However, the unitary current i was shown to increase (Beurg et al., 2006; Beurg et al., 2015; Beurg et al., 2018) from 8.3 pA to 12.1 pA when the hair cell's characteristic frequency increases from 4 kHz to 14 kHz (Beurg et al., 2006). All these currents were measured under the same experimental conditions as ours, in particular using a −80 mV holding potential and with the hair cells immersed in a standard saline containing 1.5 mM Ca^{2+}. Assuming a linear relation between the unitary current and the position of the hair cell along the tonotopic axis of the cochlea (Beurg et al., 2015; Beurg et al., 2018), we inferred the unitary currents at other cochlear locations. We then assumed that the average number of transduction channels per tip link was 2.36, as estimated in inner hair cells (Beurg et al., 2009). The number of intact tip links was then calculated as $I_{\mathrm{MAX}}/(2.36\,i)$. We performed this measurement for 10 hair cells at each cochlear location, both for inner and outer hair cells, to calculate the average number of intact tip links in any given hair cell. In these experiments, the hair cells were immersed in standard saline.

Recent measurements in the mouse cochlea have revealed that unitary currents may represent an ensemble average over multiple conductance states, raising the possibility that these currents are produced by a few (up to 5) identical transduction channels that gate cooperatively (Beurg et al., 2018). This finding does not affect our estimates, because the current that flows through a single stereocilium stays the same, whether or not it results from cooperative gating of multiple channels or from gating of an effective channel endowed with the same conductance as the total conductance of the group.

Signal Generation and Acquisition. All signals were generated and acquired under the control of a computer running a user interface programmed with LabVIEW software (version 2011, National Instruments). Command signals were produced by a 16-bit interface card at a sampling rate of 25 kHz (PCI-6733, National Instruments). A second interface card (PCI-6250, National Instruments) conducted signal acquisition with a precision of 16 bits. Sampling rates for signal generation and acquisition varied within the range 2.5–25 kHz. All signals were conditioned with an eight-pole Bessel antialiasing filter adjusted to a low-pass half-power frequency at half the sampling rate of signal acquisition.

Statistical significance. All results are quoted as mean ± standard error of the mean (n) with a number n of cells of at least 10 per group. G-Power analysis ensured that this number was sufficient to achieve a signal-to-noise ratio of 1–1.5, with 80% power at a 5% significance level. We performed a one-way ANOVA to assay statistical significance of the measured

mean-value variation of a given property, *e.g.* the hair-bundle stiffness, between the different cochlear locations for inner (IHC) or outer (OHC) hair cells. We also used two-tailed unpaired Student's *t*-tests with Welch's correction when comparing mean values between two groups of a given hair-cell type (IHC or OHC) with different characteristic frequencies or between the two cell types (IHC/OHC) with a given characteristic frequency. Stars correspond to p-values with *p < 0.05, **p < 0.01, and ***p < 0.001, whereas 'n.s.' (p > 0.05) indicates non-significant differences. To determine whether variables estimated from the product of M independent variables X_i ($i = 1 \,..\, M$) had means that were statistically different, we first calculated the standard error of the mean $\sigma_{\prod X_i}$of the product and the effective number of degrees of freedom ν_{eff} of the product. Defining $\overline{X}_i$ as the mean value of the variable X_i over n_i measurements, s_i the standard deviation and $\sigma_i = s_i/\sqrt{n_i}$ the standard error of the mean, the standard error of the mean for the product was calculated as $\sigma_{\prod X_i} = \prod \overline{X}_i \sqrt{\sum \left(\frac{\sigma_i}{\overline{X}_i}\right)^2}$ and the effective number of degrees of freedom associated with the product was calculated using the Welch-Satterthwaite approximation as $\nu_{\text{eff}} = \left[\sigma_{\prod X_i}/\prod \overline{X}_i\right]^4 / \sum \frac{1}{n_i - 1}\left(\frac{\sigma_i}{\overline{X}_i}\right)^4$. Finally, we characterized tonotopic gradients by performing weighted linear regressions, in which the weight applied to each data point was given by the inverse of the squared standard error of the mean. We then applied a *t*-test on the resulting coefficients to determine whether the observed difference between the gradients measured with inner and outer hair cells was statistically significant. The results of all statistical analyses are listed in tables associated to the main figures.

Acknowledgements:

We thank Benoît Lemaire and Rémy Fert from the machine shop of the Curie Institute, Jérémie Barral for a critical reading of the manuscript and Christine Petit for fruitful discussions. This research was supported by the French National Agency for Research (ANR-11-BSV5 0011 and ANR-16-CE13-0015) and by the Labex Celtisphybio ANR-10-LABX-0038 part of the Idex PSL. M.T. is alumnus of the Frontiers in Life Science PhD program of Université Paris Diderot and thanks the Fondation Agir pour l'Audition for a doctoral fellowship.

FIGURES AND FIGURE LEGENDS

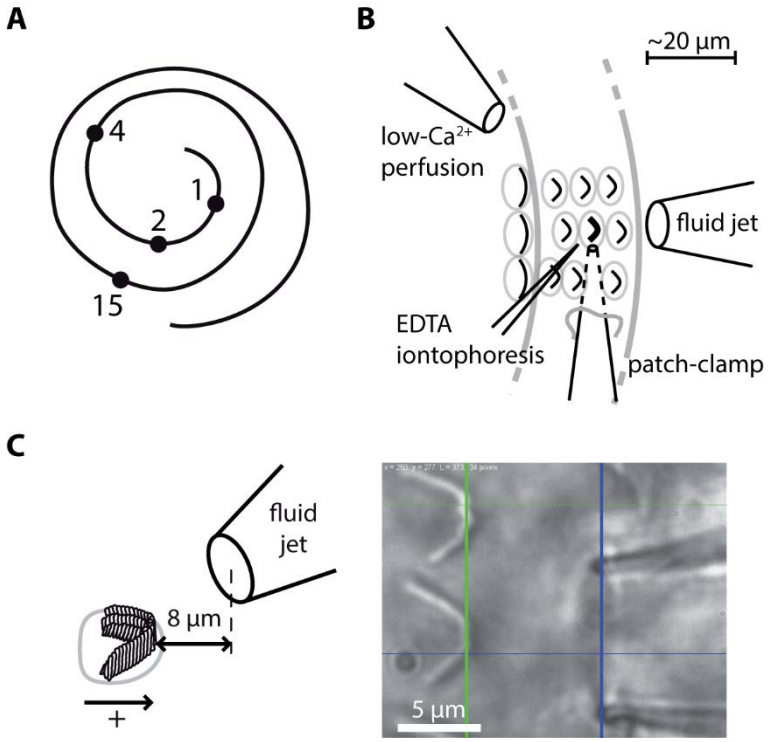

Figure 1: Hair-bundle stimulation along the tonotopic axis of the rat cochlea.

(A) Schematic representation of the tonotopic axis of the rat cochlea. Recordings were made at locations marked by black disks, corresponding to characteristic frequencies (in kHz) increasing from the apex to the base of the cochlea as indicated on the figure and to fractional distances from the apex of 5%, 10%, 20%, and 50%. The rat cochlea was typically 10 mm long. Adapted from (Viberg and Canlon, 2004). **(B)** Schematic layout of the experimental pipettes around a given outer hair cell. We combined fluid-jet stimulation of single hair bundles, iontophoresis of a Ca^{2+} chelator (EDTA), patch-clamp recordings of transduction currents, and perfusion of low-Ca^{2+} saline. **(C)** Schematic representation of the fluid-jet pipette and of a hair bundle (left) and micrograph of a fluid-jet pipette ready to stimulate an outer hair cell of the rat cochlea (right). A positive (negative) deflection of the hair bundle, as defined on the drawing, was elicited by fluid suction (ejection) into (from) the pipette, promoting opening (closure) of the transduction channels. The horizontal projected distance between the mouth of the pipette (blue vertical line) and the hair bundle (green vertical line) was set at 8 µm.

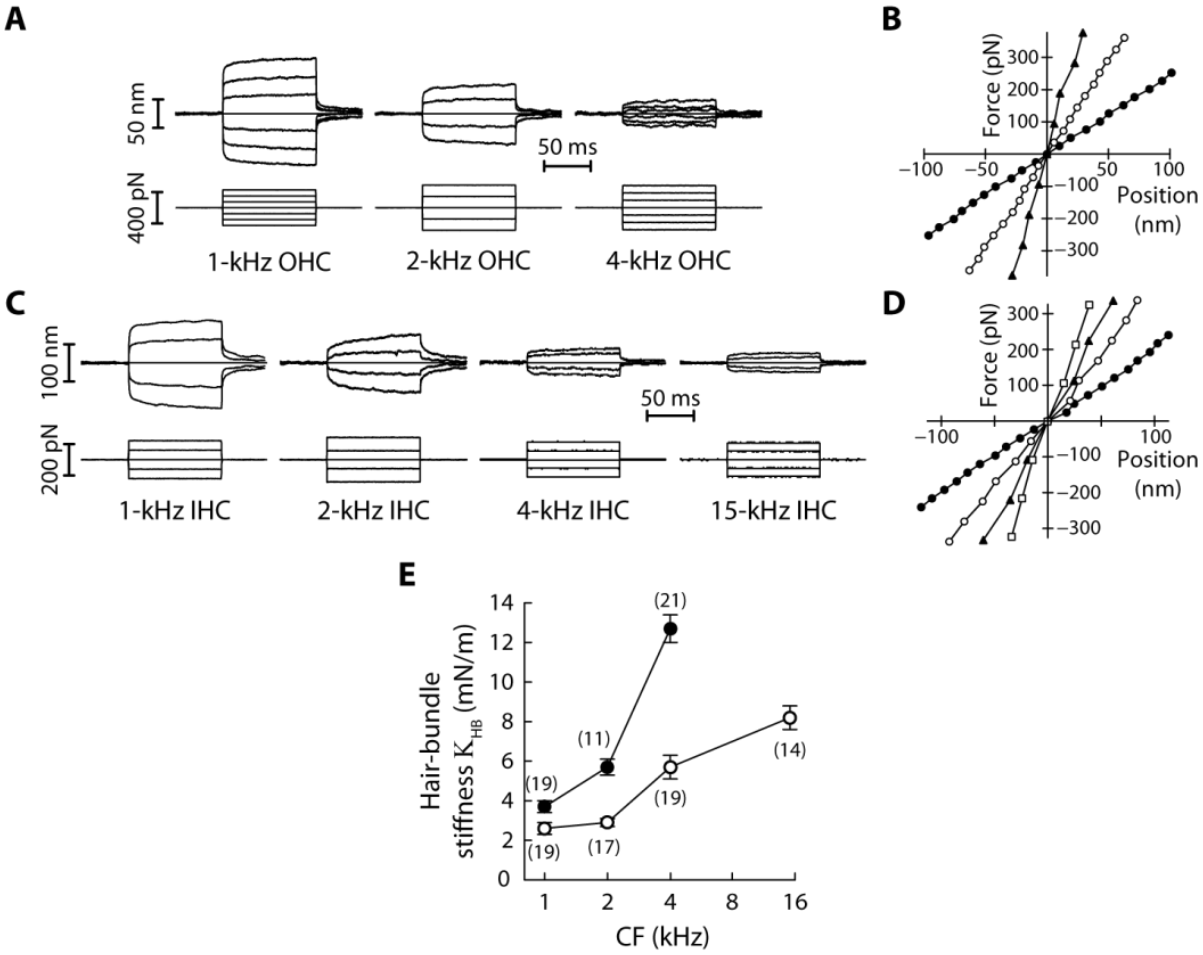

FIGURE 2: Stiffness gradients of the hair bundle.

(A) Hair-bundle movements (top) in response to series of force steps (bottom) for outer hair cells (OHC) with characteristic frequencies of 1, 2 and 4 kHz (from left to right). **(B)** Force-displacement relations for the data shown in **A**, with black disks, white disks and black triangles corresponding to characteristic frequencies of 1, 2 and 4 kHz, respectively. **(C)** Hair-bundle movements (top) in response to series of force steps (bottom) for inner hair cells (IHC) with characteristic frequencies of 1, 2, 4, and 15 kHz. **(D)** Force-displacement relations for the data shown in **C**, with black disks, white disks, black triangles, and white squares corresponding to characteristic frequencies of 1, 2, 4, and 15 kHz, respectively. **(E)** Stiffness (K_{HB}) of a hair bundle under control conditions as a function of the characteristic frequency (CF) for inner (white disks) and outer (black disks) hair cells. Each data point in **E** is the mean ± standard error of the mean (SEM) with the number of cells indicated between brackets.

The following figure and table supplements are available for figure 2:

Figure supplement 1. Velocity field of a fluid jet.

Figure supplement 2. Geometrical characteristics of a fluid jet.

688 **Figure supplement 3.** Rise time and linearity of the fluid-jet stimulus.

689 **Figure Supplement 4.** Mechanical creep during a force step.

690 **Table supplement 1.** Statistical significance.

691

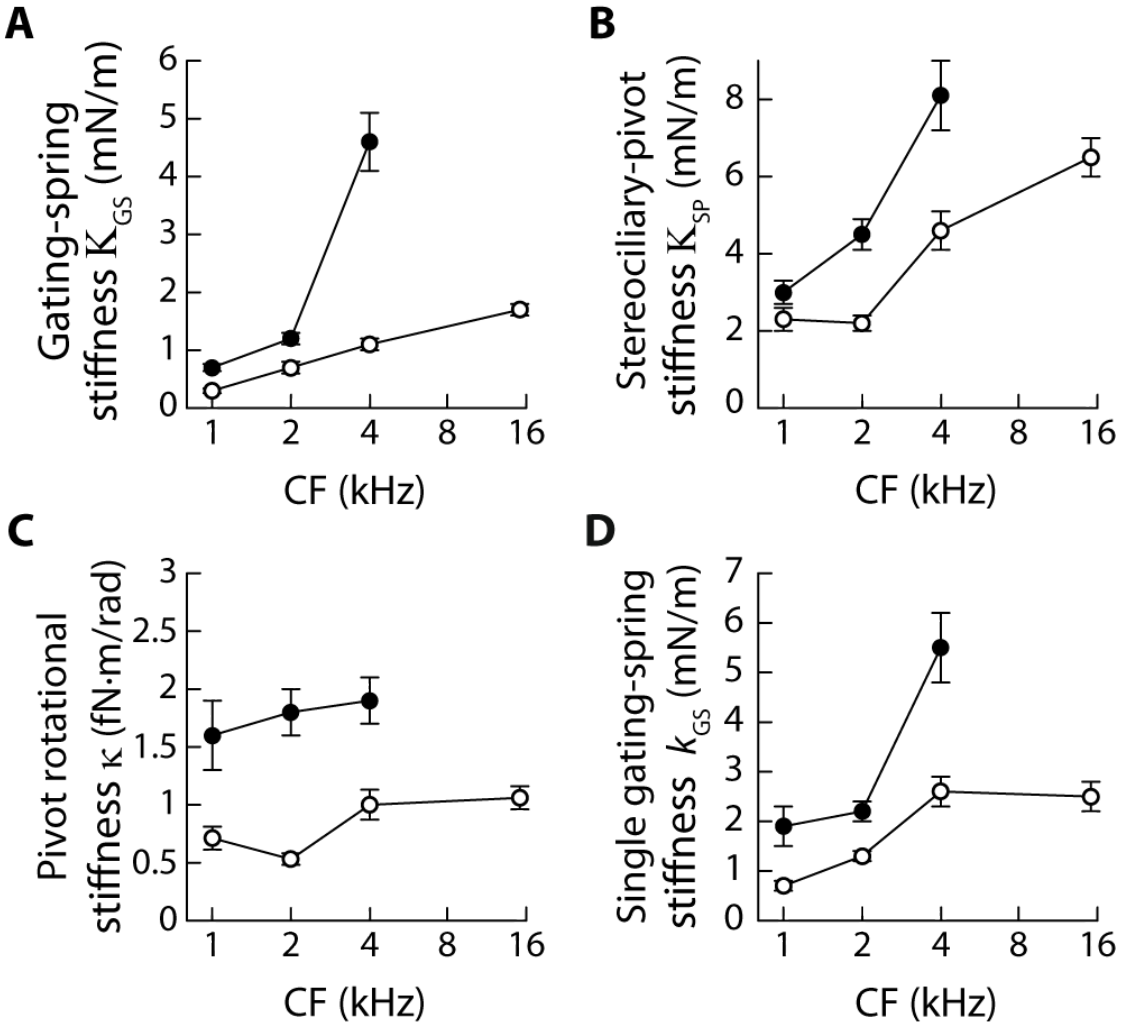

692

693 **FIGURE 3: Stiffness gradients of the gating springs and of the stereociliary pivots.**

694 Stiffness **(A)** of the contribution of the gating springs ($K_{GS} = r\, K_{HB}$), **(B)** of a hair bundle
695 after tip-link disruption, corresponding to the contribution of the stereociliary pivots ($K_{SP} =$
696 $(1 - r)\, K_{HB}$), **(C)** of a single stereociliary pivot ($\kappa = K_{SP}\, h^2/N_{SP}$), and **(D)** of a single gating
697 spring ($k_{GS} = K_{GS}\, \gamma^2/N_{TL}$) as a function of the characteristic frequency (CF) for inner (white
698 disks) and outer (black disks) hair cells. These stiffnesses were calculated from measured
699 values of the hair-bundle stiffness K_{HB} (Fig. 2), the amplitude ratio $1 - r$ of hair-bundle
700 movements before and after tip-link disruption (Figure 3–figure supplement 1), the hair-
701 bundle height h and the number of stereocilia N_{SP} (Figure 3-figure supplement 2), and the
702 average number N_{TL} of intact tip links (Figure 3–figure supplement 3). Each data point is the
703 mean ± SEM; SEMs were calculated as described in the Methods.

704 The following figure and table supplements are available for figure 3:

705 **Figure supplement 1.** Gating-spring contribution to the hair-bundle stiffness.

706 **Figure supplement 2.** Hair-bundle morphology along the tonotopic axis.

Figure supplement 3. Transduction currents and number of intact tip links along the tonotopic axis.

Table supplement 1. Morphological parameters of inner and outer hair-cell bundles.

Table supplement 2. Statistical significance.

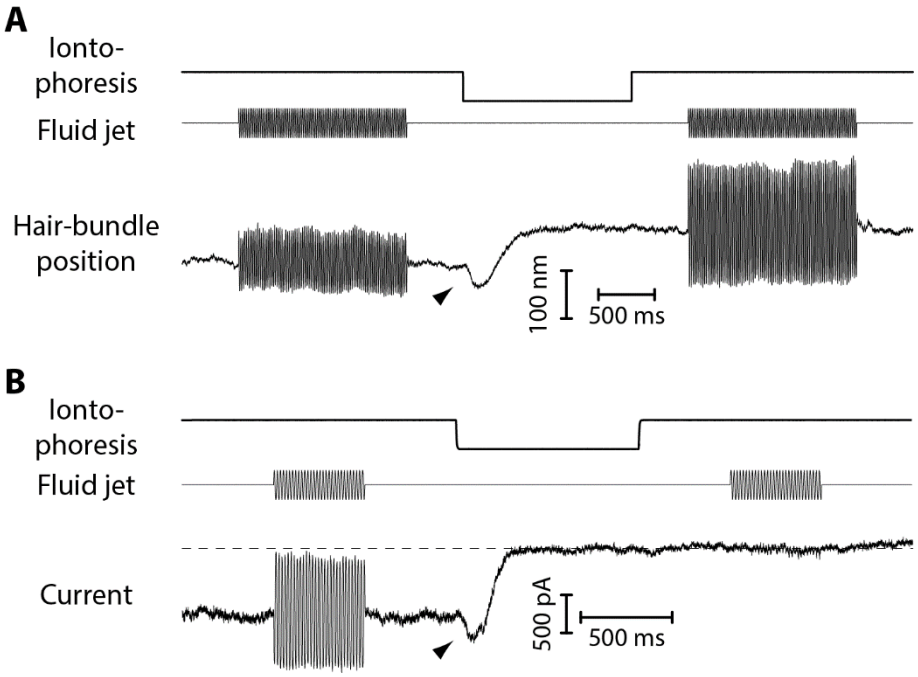

712
713

714 **FIGURE 4: Mechanical and electrical response of a hair bundle to fluid-jet stimulation**
715 **and fast calcium chelation.**

716 **(A)** An iontophoretic step of a calcium chelator (EDTA; top) elicited a biphasic movement of
717 the hair bundle from an inner hair cell (bottom): the hair bundle first moved in the negative
718 direction (arrow head) and then in the positive direction. After iontophoresis, the position
719 baseline was offset by $\Delta X_R = +78$ nm with respect to the resting position at the start of the
720 experiment. A sinusoidal command to a fluid jet (middle) evoked hair-bundle movements
721 (bottom) that increased in magnitude, here by 50%, after application of the iontophoretic step.
722 Repeating the iontophoretic step elicited no further movement and the response to fluid-jet
723 stimulation remained of the same magnitude. A similar behaviour was observed with 101
724 inner and 44 outer hair cells. **(B)** An iontophoretic step of EDTA (top) also elicited biphasic
725 variations of the transduction current: the inward current first increased (arrow head) and then
726 decreased. Before application of the calcium chelator, fluid-jet stimulation evoked a
727 transduction current of 1.5-nA peak-to-peak magnitude; the open probability of the
728 transduction channels was near ½. The transduction current was abolished by the
729 iontophoretic step. Outer hair cell at the 4-kHz location; the same behaviour was observed
730 with 17 outer hair cells. In **A-B**, the command signal to the fluid-jet device was a 60-Hz
731 sinusoid and we applied a −100-nA iontophoretic step on top of a +10-nA holding current.
732 The hair bundles were exposed to 20-µM Ca^{2+}. In **B**, the dashed line indicates the current for
733 which the transduction channels are all closed.

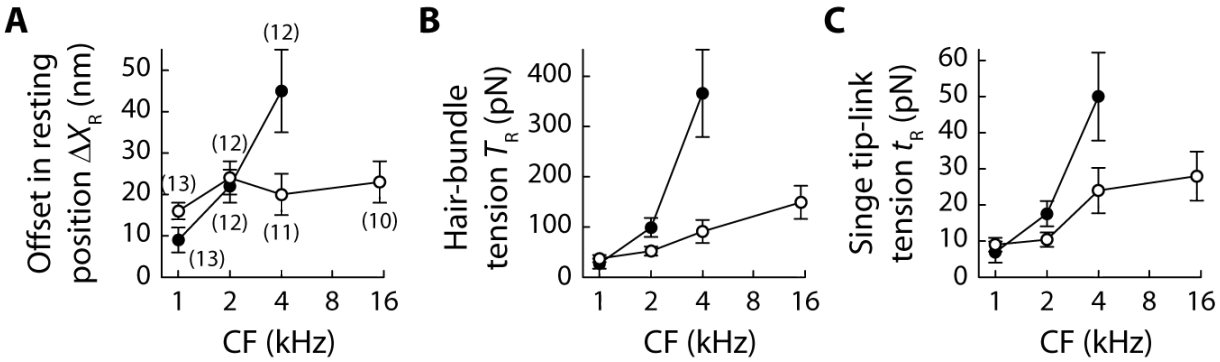

FIGURE 5: Gradients in tip-link tension at rest.

Offset ΔX_{R} in the resting position of a hair bundle resulting from tension release in the tip links **(A)**, tip-link tension $T_{\mathrm{R}} = \mathrm{K_{SP}}\,\Delta X_{\mathrm{R}}$ in the hair bundle **(B)** and tension $t_{\mathrm{R}} = T_{\mathrm{R}}/(\gamma\, N_{TL})$ along the oblique axis of a single tip link **(C)** as a function of the characteristic frequency (CF) for inner (white disks) and outer (black disks) hair cells. The hair-bundle tension T_{R} **(B)** was calculated as the product of the stereociliary-pivot stiffness $\mathrm{K_{SP}}$ shown in Fig. 3B and the data shown in **A**; this tension is estimated along the bundle's horizontal axis of mirror symmetry. The single tip-link tension t_{R} was then deduced from the projection factor γ and the average number N_{TL} of intact tip links in a hair bundle (Figure 3–figure supplement 2). Each data point in **A** is the mean ± SEM with the number of cells indicated between brackets; in **B-C**, mean values and SEMs were calculated as described in the Methods.

The following table supplement is available for figure 5:

Table supplement 1. Statistical significance.

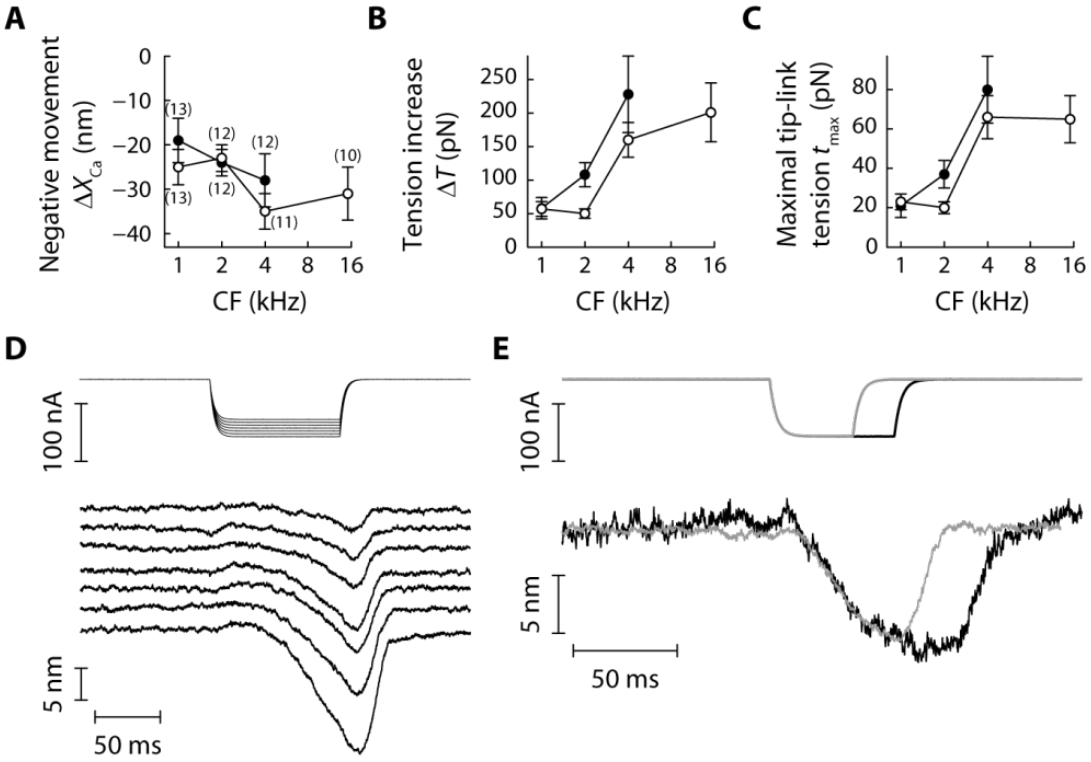

FIGURE 6: Tensioning of the tip links at decreased Ca^{2+} concentrations.

The amplitude of the negative hair-bundle movement ΔX_{Ca} **(A)**, of the maximal increase $\Delta T = -\mathrm{K_{SP}}\,\Delta X_{\mathrm{Ca}}$ in hair-bundle tension **(B)**, and of the maximal tension $t_{\max} = t_R + \Delta T/(\gamma\, N_{TL})$ in a single tip link **(C)** are plotted as a function of the hair cell's characteristic frequency (CF). The tension increase in **B** was calculated from the stiffness $\mathrm{K_{SP}}$ of the stereociliary pivots (Fig. 3B) and the data shown in **A**. The single tip-link tension $t_{\max}$ was then deduced from the tension at rest t_R in a single tip link (Fig. 5C), the projection factor γ (Figure 3–figure supplement 2) and the average number N_{TL} of intact tip links (Figure 3–figure supplement 3). **(D)** Current-step commands (top) applied to an iontopheric pipette containing the Ca^{2+} chelator EDTA evoked reversible negative movements of the hair bundle (bottom). **(E)** When the stimulus (top) was long enough, the hair bundle position could reach a steady state (bottom), corresponding to higher resting tension in the tip links. In **A-C**, the hair bundles were immersed in low-Ca^{2+} saline, for which EDTA iontophoresis led to tip-link disruption. Positions and tensions were estimated at the point of polarity reversal of the hair-bundle movement (see Fig. 4A), thus at the initiation of tip-link disruption, where the hair bundle reached its largest deflection in the negative direction and tension was thus maximal. Black and white disks correspond to outer and inner hair cells, respectively. The error bars in **A** represent ±SEM with numbers of cells indicated between brackets; in **B-C**, mean values and SEMs were calculated as described in the Methods. In **D-E**, the hair bundles

769 were immersed in a saline containing 500-µM Ca^{2+}; this higher Ca^{2+} concentration preserved
770 the integrity of the tip links upon EDTA iontophoresis.

771 The following table supplement is available for figure 6:

772 **Table supplement 1.** Statistical significance.

773

REFERENCES

Araya-Secchi R, Neel BL, Sotomayor M (2016) An elastic element in the protocadherin-15 tip link of the inner ear. Nature communications 7:13458.

Assad JA, Shepherd GM, Corey DP (1991) Tip-link integrity and mechanical transduction in vertebrate hair cells. Neuron 7:985-994.

Barral J, Jülicher F, Martin P (2018) Friction from Transduction Channels' Gating Affects Spontaneous Hair-Bundle Oscillations. Biophysical journal 114:425-436.

Bartsch TF, Hudspeth A (2018) A New Twist on Tip Links. Neuron 99:423-425.

Beurg M, Tan X, Fettiplace R (2013) A prestin motor in chicken auditory hair cells: active force generation in a nonmammalian species. Neuron 79:69-81.

Beurg M, Evans MG, Hackney CM, Fettiplace R (2006) A large-conductance calcium-selective mechanotransducer channel in mammalian cochlear hair cells. J Neurosci 26:10992-11000.

Beurg M, Nam JH, Crawford A, Fettiplace R (2008) The actions of calcium on hair bundle mechanics in mammalian cochlear hair cells. Biophys J 94:2639-2653.

Beurg M, Fettiplace R, Nam JH, Ricci AJ (2009) Localization of inner hair cell mechanotransducer channels using high-speed calcium imaging. Nat Neurosci 12:553-558.

Beurg M, Xiong W, Zhao B, Muller U, Fettiplace R (2015) Subunit determination of the conductance of hair-cell mechanotransducer channels. Proc Natl Acad Sci U S A 112:1589-1594.

Beurg M, Cui R, Goldring AC, Ebrahim S, Fettiplace R, Kachar B (2018) Variable number of TMC1-dependent mechanotransducer channels underlie tonotopic conductance gradients in the cochlea. Nat Commun 9:2185.

Bormuth V, Barral J, Joanny J-F, Juelicher F, Martin P (2014) Transduction channels' gating can control friction on vibrating hair-cell bundles in the ear. Proc Natl Acad Sci U S A 111:7185-7190.

Bosher SK, Warren RL (1978) Very low calcium content of cochlear endolymph, an extracellular fluid. Nature 273:377-378.

Bustamante C, Marko JF, Siggia ED, Smith S (1994) Entropic elasticity of lambda-phage DNA. Science 265:1599-1599.

805 Cheung EL, Corey DP (2006) Ca2+ changes the force sensitivity of the hair-cell transduction
806 channel. Biophysical journal 90:124-139.
807 Corey DP, Hudspeth AJ (1983) Kinetics of the receptor current in bullfrog saccular hair cells. J
808 Neurosci 3:962-976.
809 Corns LF, Johnson SL, Kros CJ, Marcotti W (2014) Calcium entry into stereocilia drives
810 adaptation of the mechanoelectrical transducer current of mammalian cochlear hair
811 cells. Proc Natl Acad Sci U S A 111:14918-14923.
812 Eatock RA (2000) Adaptation in hair cells. Annu Rev Neurosci 23:285-314.
813 Effertz T, Becker L, Peng AW, Ricci AJ (2017) Phosphoinositol-4,5-bisphosphate regulates
814 auditory hair cell mechanotransduction channel pore properties and fast adaptation. J
815 Neurosci.
816 Fettiplace R, Fuchs PA (1999) Mechanisms of hair cell tuning. Annu Rev Physiol 61:809-834.
817 Fettiplace R, Hackney CM (2006) The sensory and motor roles of auditory hair cells. Nat Rev
818 Neurosci 7:19-29.
819 Fettiplace R, Kim KX (2014) The physiology of mechanoelectrical transduction channels in
820 hearing. Physiological reviews 94:951-986.
821 Flock A, Strelioff D (1984) Graded and nonlinear mechanical properties of sensory hairs in
822 the mammalian hearing organ. Nature 310:597-599.
823 Freeman DM, Weiss TF (1990) Hydrodynamic analysis of a two-dimensional model for
824 micromechanical resonance of free-standing hair bundles. Hearing research 48:37-67.
825 Frishkopf LS, DeRosier DJ (1983) Mechanical tuning of free-standing stereociliary bundles
826 and frequency analysis in the alligator lizard cochlea. Hearing research 12:393-404.
827 Furness D, Katori Y, Kumar BN, Hackney C (2008) The dimensions and structural attachments
828 of tip links in mammalian cochlear hair cells and the effects of exposure to different
829 levels of extracellular calcium. Neuroscience 154:10-21.
830 Ge J, Elferich J, Goehring A, Zhao H, Schuck P, Gouaux E (2018) Structure of mouse
831 protocadherin 15 of the stereocilia tip link in complex with LHFPL5. eLife 7.
832 Géléoc GS, Lennan GW, Richardson GP, Kros CJ (1997) A quantitative comparison of
833 mechanoelectrical transduction in vestibular and auditory hair cells of neonatal mice.
834 Proc R Soc Lond B 264:611-621.
835 Gillespie PG, Muller U (2009) Mechanotransduction by hair cells: models, molecules, and
836 mechanisms. Cell 139:33-44.

837 Greenwood DD (1990) A cochlear frequency-position function for several species—29 years
838 later. The Journal of the Acoustical Society of America 87:2592-2605.
839 Gummer AW, Hemmert W, Zenner HP (1996) Resonant tectorial membrane motion in the
840 inner ear: its crucial role in frequency tuning. Proc Natl Acad Sci USA 93:8727-8732.
841 Hacohen N, Assad J, Smith W, Corey D (1989) Regulation of tension on hair-cell transduction
842 channels: displacement and calcium dependence. Journal of Neuroscience 9:3988-3997.
843 Happel J, Brenner H (2012) Low Reynolds number hydrodynamics: with special applications
844 to particulate media: Springer Science & Business Media.
845 Holton T, Hudspeth AJ (1983) A micromechanical contribution to cochlear tuning and
846 tonotopic organization. Science 222:508-510.
847 Howard J, Hudspeth A (1988) Compliance of the hair bundle associated with gating of
848 mechanoelectrical transduction channels in the bullfrog's saccular hair cell. Neuron
849 1:189-199.
850 Hudspeth AJ (1989) How the ear's works work. Nature 341:397-404.
851 Hudspeth AJ (2008) Making an effort to listen: mechanical amplification in the ear. Neuron
852 59:530-545.
853 Hudspeth AJ (2014) Integrating the active process of hair cells with cochlear function. Nature
854 reviews Neuroscience 15:600-614.
855 Hudspeth AJ, Gillespie PG (1994) Pulling springs to tune transduction: adaptation by hair
856 cells. Neuron 12:1-9.
857 Hudspeth AJ, Julicher F, Martin P (2010) A critique of the critical cochlea: Hopf--a bifurcation-
858 -is better than none. Journal of neurophysiology 104:1219-1229.
859 Indzhykulian AA, Stepanyan R, Nelina A, Spinelli KJ, Ahmed ZM, Belyantseva IA, Friedman TB,
860 Barr-Gillespie PG, Frolenkov GI (2013) Molecular remodeling of tip links underlies
861 mechanosensory regeneration in auditory hair cells. PLoS biology 11:e1001583.
862 Jaramillo F, Hudspeth AJ (1993) Displacement-clamp measurement of the forces exerted by
863 gating springs in the hair bundle. Proc Natl Acad Sci U S A 90:1330-1334.
864 Johnson SL, Beurg M, Marcotti W, Fettiplace R (2011) Prestin-driven cochlear amplification is
865 not limited by the outer hair cell membrane time constant. Neuron 70:1143-1154.
866 Kachar B, Parakkal M, Kurc M, Zhao Y, Gillespie PG (2000) High-resolution structure of hair-
867 cell tip links. Proc Natl Acad Sci USA 97:13336-13341.

868 Kang H, Wen Q, Janmey PA, Tang JX, Conti E, MacKintosh FC (2009) Nonlinear elasticity of
869 stiff filament networks: strain stiffening, negative normal stress, and filament alignment
870 in fibrin gels. The Journal of Physical Chemistry B 113:3799-3805.
871 Kazmierczak P, Sakaguchi H, Tokita J, Wilson-Kubalek EM, Milligan RA, Muller U, Kachar B
872 (2007) Cadherin 23 and protocadherin 15 interact to form tip-link filaments in sensory
873 hair cells. Nature 449:87-91.
874 Kennedy HJ, Crawford AC, Fettiplace R (2005) Force generation by mammalian hair bundles
875 supports a role in cochlear amplification. Nature 433:880-883.
876 Kennedy HJ, Evans MG, Crawford AC, Fettiplace R (2003) Fast adaptation of
877 mechanoelectrical transducer channels in mammalian cochlear hair cells. Nat Neurosci
878 6:832-836.
879 Kennedy HJ, Evans MG, Crawford AC, Fettiplace R (2006) Depolarization of cochlear outer
880 hair cells evokes active hair bundle motion by two mechanisms. Journal of Neuroscience
881 26:2757-2766.
882 Kros CJ, Rusch A, Richardson GP (1992) Mechano-electrical transducer currents in hair cells
883 of the cultured neonatal mouse cochlea. Proceedings Biological sciences / The Royal
884 Society 249:185-193.
885 Leith D (1987) Drag on Nonspherical Objects. Aerosol Science and Technology 6:153-161.
886 Lewis ER, Leverenz EL, Koyama H (1982) The tonotopic organization of the bullfrog
887 amphibian papilla, an auditory organ lacking a basilar membrane. Journal of
888 comparative physiology 145:437-445.
889 Lim DJ (1986) Functional structure of the organ of Corti: a review. Hear Res 22:117-146.
890 Manley GA, Yates GK, Köppl C (1988) Auditory peripheral tuning: evidence for a simple
891 resonance phenomenon in the lizard Tiliqua. Hearing research 33:181-189.
892 Markin VS, Hudspeth AJ (1995) Gating-spring models of mechanoelectrical transduction by
893 hair cells of the internal ear. Annu Rev Biophys Biomol Struct 24:59-83.
894 Marquis RE, Hudspeth AJ (1997) Effects of extracellular Ca2+ concentration on hair-bundle
895 stiffness and gating-spring integrity in hair cells. Proc Natl Acad Sci USA 94:11923-11928.
896 Martin P (2008) Active hair-bundle motility of the hair cells of vestibular and auditory organs.
897 In: Active processes and otoacoustic emissions in hearing (Manley GA, Popper AN, Fay
898 RR, eds), pp 93-143. New York: Springer.

899 Martin P, Hudspeth AJ, Jülicher F (2001) Comparison of a hair bundle's spontaneous
900 oscillations with its response to mechanical stimulation reveals the underlying active
901 process. Proc Natl Acad Sci USA 98:14380-14385.
902 Michalski N, Petit C (2015) Genetics of auditory mechano-electrical transduction. Pflügers
903 Archiv-European Journal of Physiology 467:49-72.
904 Peng AW, Effertz T, Ricci AJ (2013) Adaptation of mammalian auditory hair cell
905 mechanotransduction is independent of calcium entry. Neuron 80:960-972.
906 Peng AW, Gnanasambandam R, Sachs F, Ricci AJ (2016) Adaptation Independent Modulation
907 of Auditory Hair Cell Mechanotransduction Channel Open Probability Implicates a Role
908 for the Lipid Bilayer. J Neurosci 36:2945-2956.
909 Peng AW, Belyantseva IA, Hsu PD, Friedman TB, Heller S (2009) Twinfilin 2 regulates actin
910 filament lengths in cochlear stereocilia. Journal of Neuroscience 29:15083-15088.
911 Pickles J, Comis S, Osborne M (1984) Cross-links between stereocilia in the guinea pig organ
912 of Corti, and their possible relation to sensory transduction. Hearing research 15:103-
913 112.
914 Ricci A, Crawford A, Fettiplace R (2002) Mechanisms of active hair bundle motion in auditory
915 hair cells. Journal of Neuroscience 22:44-52.
916 Ricci AJ, Wu YC, Fettiplace R (1998) The endogenous calcium buffer and the time course of
917 transducer adaptation in auditory hair cells. J Neurosci 18:8261-8277.
918 Ricci AJ, Crawford AC, Fettiplace R (2003) Tonotopic variation in the conductance of the hair
919 cell mechanotransducer channel. Neuron 40:983-990.
920 Ricci AJ, Kennedy HJ, Crawford AC, Fettiplace R (2005) The transduction channel filter in
921 auditory hair cells. J Neurosci 25:7831-7839.
922 Rief M, Gautel M, Oesterhelt F, Fernandez JM, Gaub HE (1997) Reversible unfolding of
923 individual titin immunoglobulin domains by AFM. science 276:1109-1112.
924 Roth B, Bruns V (1992) Postnatal development of the rat organ of Corti. II. Hair cell receptors
925 and their supporting elements. Anat Embryol 185:571-581.
926 Russell I, Sellick P (1983) Low-frequency characteristics of intracellularly recorded receptor
927 potentials in guinea-pig cochlear hair cells. The Journal of Physiology 338:179-206.
928 Russell IJ, Kössl M, Richardson GP (1992) Nonlinear mechanical responses of mouse cochlear
929 hair bundles. Proc R Soc Lond B 250:217-227.

930 Schlichting VH (1933) Laminare strahlausbreitung. ZAMM-Journal of Applied Mathematics
931 and Mechanics/Zeitschrift für Angewandte Mathematik und Mechanik 13:260-263.
932 Tilney LG, Tilney MS (1988) The actin filament content of hair cells of the bird cochlea is
933 nearly constant even though the length, width, and number of stereocilia vary
934 depending on the hair cell location. The Journal of cell biology 107:2563-2574.
935 Tilney LG, Tilney MS, DeRosier DJ (1992) Actin filaments, stereocilia, and hair cells: how cells
936 count and measure. Annual review of cell biology 8:257-274.
937 Tinevez JY, Julicher F, Martin P (2007) Unifying the various incarnations of active hair-bundle
938 motility by the vertebrate hair cell. Biophysical journal 93:4053-4067.
939 Tirado MM, Torre JGdl (1979) Translational friction coefficients of rigid, symmetric top
940 macromolecules. Application to circular cylinders. The Journal of Chemical Physics
941 71:2581-2587.
942 Turner RG, Muraski AA, Nielsen DW (1981) Cilium length: influence on neural tonotopic
943 organization. Science.
944 Viberg A, Canlon B (2004) The guide to plotting a cochleogram. Hear Res 197:1-10.
945 Vilfan A, Duke T (2003) Two adaptation processes in auditory hair cells together can provide
946 an active amplifier. Biophysical journal 85:191-203.
947 Waguespack J, Salles FT, Kachar B, Ricci AJ (2007) Stepwise morphological and functional
948 maturation of mechanotransduction in rat outer hair cells. J Neurosci 27:13890-13902.
949 Wright A (1984) Dimensions of the cochlear stereocilia in man and the guinea pig. Hear Res
950 13:89-98.

951